ADVANCED MATERIALS
www.advmat.de

www.MaterialsViews.com

Design Principles for Heteroatom-Doped Carbon Nanomaterials as Highly Efficient Catalysts for Fuel Cells and Metal–Air Batteries

*Zhenghang Zhao, Mingtao Li, Lipeng Zhang, Liming Dai, and Zhenhai Xia**

Clean and sustainable energy technologies, such as fuel cells, metal–air batteries, and water-splitting, are currently under intensive research and development because of their high efficiency, promising large-scale applications, and virtually no pollution or greenhouse gas emission.[1] At the heart of these energy devices, there are two critical chemical reactions: oxygen reduction reaction (ORR) and oxygen evolution reaction (OER) that determine the efficiencies of energy conversion and storage. These reactions, however, are sluggish and require noble metal catalysts (e.g., platinum).[2] The limited resources and high cost of platinum have hampered the commercialization of these technologies. While facing a prohibitively high cost, the Pt-based electrode also suffers from other problems, such as low selectivity, poor durability, and detrimental environmental effects.[3] Therefore, it is necessary to search for alternative materials that are earth-abundant, cost-effective, and can show catalytic activities comparable to or even higher than that of noble metal catalysts for ORR and OER.

Carbon nanomaterials, such as carbon nanotubes (CNTs) and graphene, are appealing for metal-free catalytic applications because of their potentially low cost, unique molecular structures with a large surface area and catalytic activities, excellent mechanical, thermal, and electrical properties, and high stability in both acidic and alkaline environments.[4–6] Furthermore, doping with p-block elements in the periodic table can effectively modify the electronic structures of carbon nanomaterials to facilitate ORR and OER. Therefore, extensive work has been carried out to search for efficient carbon-based catalysts for energy conversion and storage.[6–23] Although the superior catalytic capabilities of heteroatom-doped carbon nanomaterials for ORR have been demonstrated, trial-and-error approaches are still used to date for the development of highly efficient catalysts. To rationally design a catalyst, it is critical to understand which intrinsic material characteristics, or descriptors, control catalysis. The development of design principles or descriptors that correlate doped structures to the catalytic activity of carbon-based catalysts will accelerate the search for metal-free highly active catalysts based on earth-abundant, cost-effective materials to replace noble metals, including platinum.

Recently, it was proposed that the energy level of a metal atom's d-band center could serve as the activity descriptor for metal surfaces,[24] and similarly, e_g-filling acts as a descriptor for transition-metal-oxide perovskites.[25] For the entire family of metal-free carbon-based catalysts, however, there is a lack of an intrinsic descriptor that governs catalytic activities, which hinder the rational design of catalysts with desirable properties. Although a descriptor similar to the d-band theory was proposed for heteroatom-doped graphene[26] and the work functions of the doped carbon, measured by Kelvin probe force microscopy, displayed a strong correlation with the ORR activity,[27] the volcano relationship seems to be yet established for ORR and OER. In this study, we have, for the first time, identified a material property that serves as the activity descriptor for predicating bifunctional ORR/OER activities, and established a volcano relationship between the descriptor and the intrinsic bifunctional activity of heteroatom-doped carbon-based catalysts. Such descriptor enables us to design new metal-free catalysts with enhanced ORR/OER activities, even better than those reported for platinum-based metal catalysts. As supported by a large number of reports for ORR activity of p-block element doped carbon nanomaterials,[6–10] this descriptor can also be used as a powerful guidance to develop various new earth-abundant, cost-effective catalyst materials.

Overpotential U in ORR/OER is an important measure of intrinsic catalytic activities of a catalyst.[28] An ideal catalyst should be able to facilitate oxygen reduction or water oxidation just above the equilibrium potential (U^0), with zero overpotential ($U = 0$). However, the ideal case cannot be achieved in general because the binding energies of the intermediates are correlated.[29] Therefore, thermodynamically, a catalyst with lower U would have better performance. To rationally search for the best catalyst of carbon nanomaterials (e.g., graphene and CNTs), we calculated the free energy and overpotential for elementary reactions of ORR/OER (Equations (S1)–(S23), Supporting Information) for all the possible active sites on graphene structures doped with p-block elements, X (X = N, B, P, S, Si, Se, Sb, F, Cl,

Z. Zhao, Dr. L. Zhang, Prof. Z. H. Xia
Department of Materials Science and Engineering
Department of Chemistry
University of North Texas
Denton, TX 76203, USA
E-mail: zhenhai.xia@unt.edu

Dr. M. Li
International Research Center for Renewable Energy
State key Laboratory of Multiphase Flow in Power Engineering
Xi'an Jiaotong University
Xi'an, Shaanxi 710049, P. R. China

Prof. L. M. Dai
Center of Advanced Science and Engineering for Carbon (Case4Carbon)
Department of Macromolecular Science and Engineering
Case Western Reserve University
Cleveland, OH 44106, USA

Prof. Z. H. Xia
School of Materials Science and Engineering
Northwestern Polytechnical University
Xi'an, Shaanxi 710072, P. R. China

DOI: 10.1002/adma.201503211

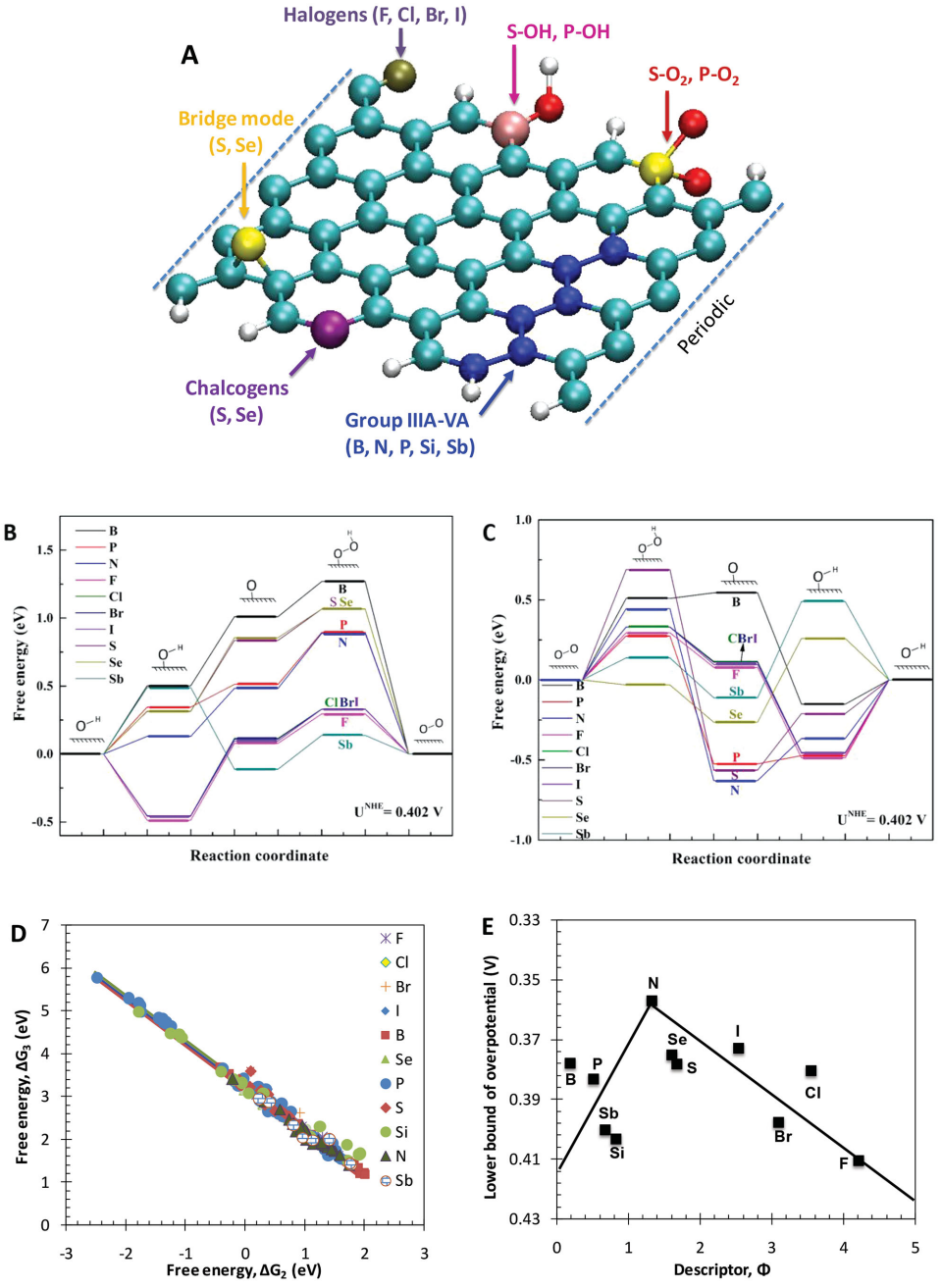

Figure 1. A) Schematic of the X-doped graphene nanoribbons, showing the possible positions of dopants. Free energy diagram of X-doped graphene nanoribbons with the best catalytic performance at the equilibrium potential ($U^0 = 0.402$ V) for B) OER and C) ORR in alkaline medium. D) Reaction energies of the third electron transfer, ΔG_3 (Equation (S20), Supporting Information) versus the second electron transfer, ΔG_2, (Equation (S19), Supporting Information) on different sites of armchair and zigzag graphene nanoribbons for OER in alkaline medium. E) The lower limit of OER/ORR overpotentials for X-doped graphene structures versus descriptor Φ.

Br, I, POH, SOH, PO_2, SeO_2, and SO_2, etc.), and determined the rate-limiting step by selecting the maximum overpotentials in the elementary reaction steps (materials and methods for free energy and overpotential calculations are described in detail in the Supporting Information). The doping positions in each structure were changed with respect to the graphene edge to reveal the effect of doping sites (**Figure 1**A and Figure S1, Supporting Information). Free energy diagrams (Figure 1B and Figure S2a, Supporting Information) indicate that the third step (Equation (S20), Supporting Information) in OER is the rate-limiting step for X-doped structures. Figure 1D shows the free energy of OER in the third electron transfer (Equation (S20), Supporting Information) versus the second one (Equation (S19), Supporting Information) for X-doped graphene structures in alkaline media. The free energies of the third reaction of OER is linearly related to that of the second one by $\Delta G_3 = -\Delta G_2 + C_X$,

where the constant C_X depends on dopant type X, but is independent of the binding strength to the surface. Thus, a lower limit of OER overpotential (Table S1, Supporting Information) can be determined from the relationship. Taking N-doped graphene structure as an example, $\Delta G_2 + \Delta G_3 = C_N = 1.568$ eV. When $\Delta G_2 = \Delta G_3 = 0.759$ eV, the OER overpotential has the lower limit, $U_{limit}^{OER} = 0.759 - 0.402 = 0.357$ V. Similarly, the first or last step of ORR (Equation (S14) or (S17), Supporting Information) is the rate-limiting reaction for all the doped structures (Figure 1C and Figure S2b, Supporting Information), and $\Delta G_4 + \Delta G_1 = 1.603 - C_X$. The lower limit of ORR overpotential U_{limit}^{ORR} can then be derived, which is the same as that for OER. Note that from Table S1 (Supporting Information), U_{limit} predicted for those dopants are much lower than that of noble metal catalysts (≈0.45 V for ORR on Pt[28] and ≈0.42 V for OER on RuO_2,[29] indicating the potential of p-block element-doped carbon nanomaterials as efficient catalysts for fuel cells and metal–air batteries.

To identify an ORR/OER activity descriptor for the p-block element-doped graphene structures, we began by examining the relationship between the activity and the intrinsic properties of dopants. It is well known that the electronegativity E_X represents the ability to acquire electron when a covalent bond is formed whereas the electron affinity A_X, is the energy given off when a neutral atom gains an extra electron to form a negatively charged ion in the chemical reaction. The difference in these characteristics between the dopants and carbon may strongly influence the electron transfer and reaction energy in ORR and OER. Thus, we introduce a simple descriptor: $\Phi = (E_X/E_C) \times (A_X/A_C)$, a dimensionless factor, to represent the effect of these characteristics. Plotting ORR activity (overpotential) as a function of Φ produces a definitive volcano plot (Figure 1E) with nitrogen sitting on the summit of the volcano in a good consistence with reported experimental data.[6–22] Therefore, the product of relative electronegativity and electron affinity is identified as a descriptor for the ORR/OER activity of p-block element-doped carbon materials.

The lower bound of overpotential U_{limit} represents the most desirable state that a catalyst could reach. We further calculated overpotentials of all the elementary reaction steps for all the doped structures, from which the minimum ORR and OER overpotentials (U_{min}^{ORR} and U_{min}^{OER}) were determined for all types of dopants (Table S2, Supporting Information). **Figure 2**A,B show the plots of the U^{ORR} and U^{OER} versus energy adsorption for all the possible active sites of the doped carbon nanostructures. For all types of dopants, the overpotentials exhibit volcano relationship against descriptors, adsorption free energy $\Delta G_{O^*-OH^*}$ for OER, and ΔG_{OH^*} for ORR. Although these descriptors well correlate the ORR/OER activity with the adsorption free energy of intermediates, OOH*, O*, and OH*, they do not link intrinsic materials properties to the activities. We have calculated the adsorption free energy of intermediates on the most

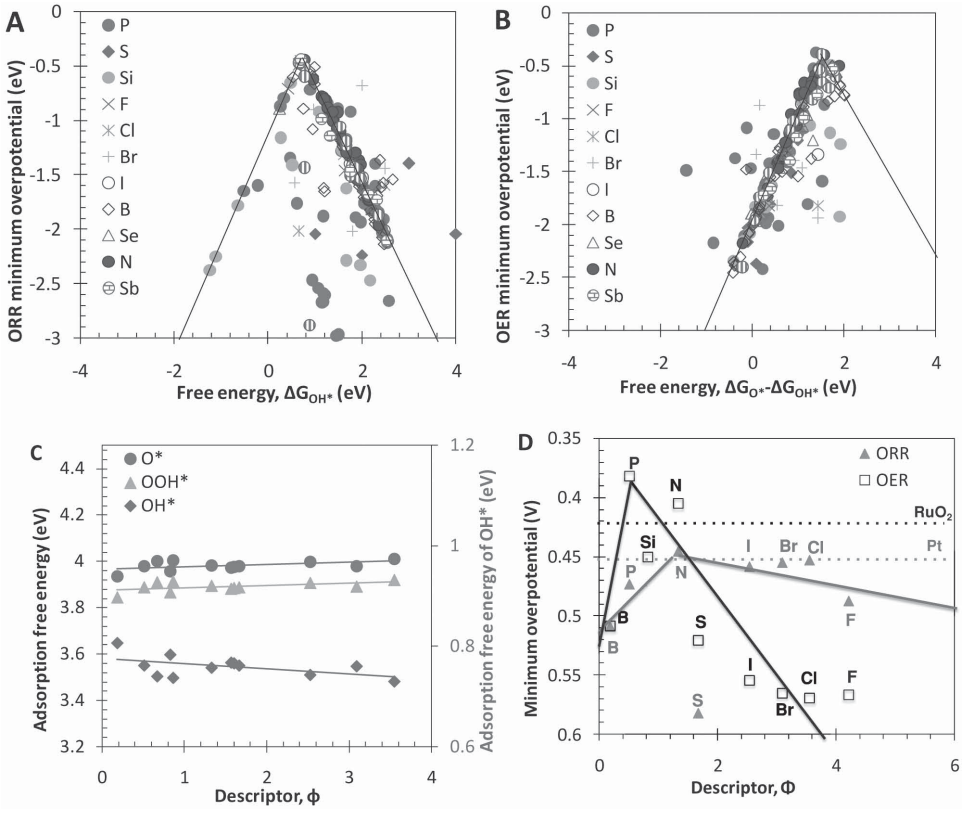

Figure 2. A) ORR overpotential versus adsorption free energies ΔG_{OH^*}, B) OER overpotential versus adsorption free energy ΔG_{O^*}–ΔG_{OH^*} on different sites of graphene nanoribbons, C) adsorption free energy of OOH*, OH*, and O* as a function of the descriptor Φ, and D) minimum ORR/OER overpotential versus the descriptor Φ for X-doped graphene. The overpotentials of the best catalysts predicted theoretically for ORR (Pt)[28] and OER (RuO_2)[29] are also plotted in (D).

desirable active sites of X-doped graphene materials with the lower limit of overpotentials, and found that the energy changes linearly with the descriptor Φ (Figure 2C). Therefore, Φ can be a simple activity descriptor suitable for metal-free doped nanocarbon catalysts that could also lead to a correlation between the binding strength and ORR/OER activity. Applying Φ to the X-doped carbon structures with the best performance yields a volcano relationship for U_{min} versus Φ, as shown in Figure 2D. Again, nitrogen was identified as the best dopant in graphene for ORR, whereas phosphorus exhibited the lowest overpotential for OER. When Φ_{ORR} = 1–3 and Φ_{OER} = 0.5–2, the activities of doped carbon could exceed the best catalysts, Pt for ORR and RuO_2 for OER, respectively,[28,29] indicating that p-orbital element, in particular N and P, doped (or codoped) graphene can be bifunctional catalysts with the performance better than their noble-metal counterparts.

To verify the descriptor, we compared the predictions with the ORR catalytic activity measured in linear scan voltammogram (LSV) experiments. It is well known that the limiting current from LSV measurements well represents the ORR catalytic activity of electrocatalysts, whereas onset potential is more corresponding to the theoretically obtained minimum overpotential. We cited the data reported for p-element-doped graphene and CNTs.[6–22,30] and made plots of the current density and onset potential versus the descriptor. To reliably compare the data from different sources, the current density is normalized by the benchmarked Pt/C electrode current density measured under the same condition in the same experiment, while the onset potential relative to that of Pt/C electrode in the same experiment is used (refer to relative onset potential). Apart from doping elements, other factors such as surface area and morphology of the materials and dopant content could also affect the catalytic activities. Since only graphene and CNTs are selected, their morphology and dopant content are similar and comparable. To further minimize the possible surface area/morphology/dopant content effects, we have averaged the data that were carefully selected from the literature. **Figure 3**A shows the normalized current of p-element-doped carbon nanomaterials as a function of the descriptor. Clearly, the experimental results show a volcano relationship with nitrogen sitting on its top. This volcano relationship is consistent with the predictions from our calculations, as shown in Figure 2D. Similar volcano relationship between the onset potential and Φ is also demonstrated for the p-block elements except for fluorine (Figure 3B). The unusual onset potential of fluorine may be attributed to unexplored ORR mechanisms because of its extremely high reactivity. Anyway, the experimental data support that the primary descriptor governs the ORR activity of the p-element-doped carbon nanomaterials, as demonstrated theoretically in this work.

The most active catalytic sites on the doped graphene were identified for all the dopants, as shown in Figure S3 (Supporting Information). The elementary reactions of ORR on the most active sites of the graphene nanoribbons are shown in Figures S4–S8 (Supporting Information). Overall, the active catalytic centers created by doping with all the p-elements are carbon atoms near the dopants. Those elements with $\Phi < 1$ (e.g., B, P, Si, and Sb) themselves can act as ORR active centers (Figure 3C) while the dopants with $\Phi > 1$ (N, S, Se, and halogen) cannot do so. In the case of X–O_2 and X–OH doping, the active sites are dopants themselves (Figures S6 and S7, Supporting Information). Interestingly, N-doping can result in two most active ORR and OER catalytic centers near the dopant in the same N-doped structure (Figure 3D), whereas doping with halogen elements creates ORR/OER center at the same spot (Figure 3E). These results suggest that the doped carbon nanomaterials can be bifunctional catalysts with high activities. This may be attributable to the electron accepting/donating nature of the doping elements relative to carbon.[21,31] As shown in Figure S9 (Supporting Information), the dopants with $\Phi < 1$ result in positive charge on themselves as well as on their neighboring carbon atoms, while those with $\Phi > 1$ induce negative charge on themselves and positive charge on neighboring carbon atoms. These positive charged atoms create active centers for catalyzing ORR and/or OER.

The proposed active descriptor has predictive power for p-block element doped carbon nanomaterials. Using the descriptor Φ, therefore, we can further predict the catalytic activities of other p-block element dopants. According to their value of Φ, these unexplored p-elements can be divided into three groups: Group I with Φ similar to B, including Tl, Pb, In, Al, Ga, and Ge; Group II with a value of Φ close to P, including As, Bi, and Sn; and Group III (Po, Te, and At) with $\Phi > 1$. As shown in Figure 3A, the activity of dopants from Groups I and II will be similar to B and P, respectively, and dopants themselves could be an active site for ORR and OER. The third groups will have relatively high activity with respect to Pt.

In addition to the types of dopants, the locations of dopants also strongly affect the catalytic activity of the doped carbon. We have determined the lowest overpotential of active centers as a function of the distance between the dopant and the active centers (Figure S10a, Supporting Information). The overpotential remains relatively low within a critical distance of d_c ≈3 Å and gradually increases beyond the critical distance. Thus, a single dopant can effectively induce more active sites within ≈3 Å for catalyzing ORR and OER. Figure S10b (Supporting Information) shows the overpotential versus the distance from active sites to graphene edge. The overpotential is relatively low within the distance of ≈3 Å, but it increases beyond this range. Also shown in Figure S10b (Supporting Information), active sites with low overpotential distribute near the graphene edge. Similarly, the overpotentials increase with increasing the distance from the dopants to the edge (Figure S10c, Supporting Information). Therefore, the graphene edge seems critical to the catalytic activities of all the dopants studied in this work. Experimentally, the graphene edge has been recently demonstrated to show a much faster electron transfer rate and higher electrocatalytic activity than those of the graphene basal plane.[32] Therefore, the graphene edge could be an ideal doping side for efficient electrocatalysis.[17,32,33] In most cases, the most active OER and ORR centers locate within a distance of 3 Å near the edge of the graphene. This distance is identical to d_c, as well as the distance of edge effect identified in graphene nanoribbons.[34] Thus, the high OER/ORR activities can be achieved by doping p-orbital atoms near the edge within the distance of the edge effect. Such a feature of the doped nanocarbons can be used to enhance ORR/OER activities of carbon-based catalysts in the fuel cells and metal–air batteries.

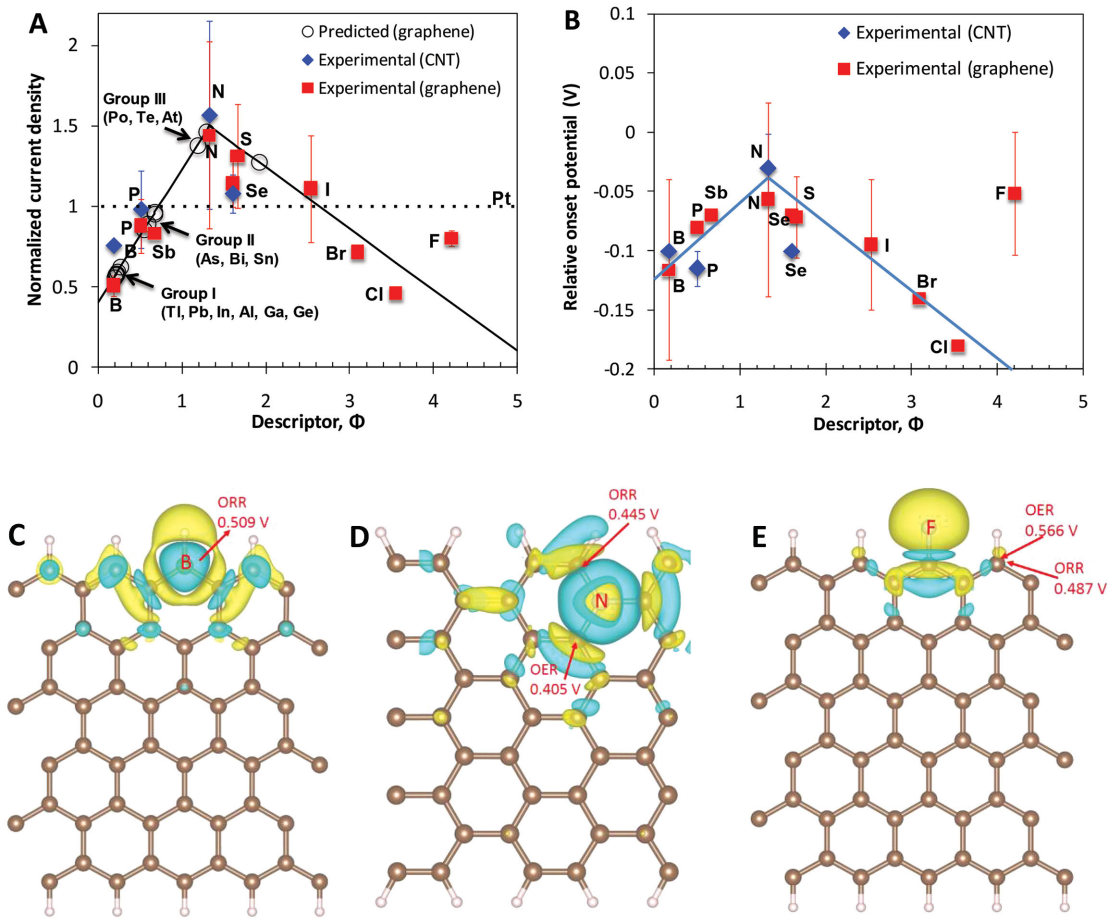

Figure 3. A) Measured limiting current density from the LSV curves, normalized by Pt/C electrode current density at 0.5 V (SCE, saturated calomel electrode) under the same conditions in the same experiment, and the predictions, and B) measured relative onset potential (difference between the doped carbon nanomaterials and the Pt/C electrode), as a function of descriptor, Φ for p-element-doped carbon nanomaterials. The average current density is cited for graphene doped with B,[4,8] P,[10,35] N,[6,12,15] S,[13] F,[14,15,36] Cl,[17] Br,[17] I,[17,19] Se,[20] and Sb,[22] and for CNT doped with B,[9] P,[11,18] N,[16,18,21,30,37] and Se.[20] The predictions are based on the fitting lines of the experimental results. Differential charge density distributions (between doped and undoped graphene) of C) boron, D) nitrogen, and E) fluorine doped graphene sheets. The active sites with the minimum overpotential are marked with values. Yellow and blue colors indicate the positive and negative values of electron quantities, respectively. The isosurface value is set to 0.0015. Brown and white balls refer to carbon and hydrogen atoms, respectively.

The success of the descriptor stems from its ability to capture the major characteristics of p-block element-doped carbon nanomaterials. The elements in the p-block of the periodic table have unique electronic structures (p molecular orbitals in the outermost shell, or valence orbital level) similar to carbon, and have relatively large electronegativities and electron affinity. Since most carbon nanomaterials consist of graphitic (graphene) structures, doping the p-block elements can provide extra p-electrons to the carbon conjugated system to induce electron-donating/accepting sites, depending on the difference in electronegativity and affinity between carbon and dopants. As shown in Figures S3 and S9 (Supporting Information), p-doping results in charge redistribution on carbon surface, in particular near dopants. The redistribution of p-orbital electron induced by doping could facilitate intermediate adsorption and electron transfers between the doped carbon materials and the reaction intermediates in the ORR/OER.

The new descriptor has an intrinsic relationship with the intermediate adsorption, and therefore the catalytic activities. Recently, Jiao et al.[26] investigated the origin of the binding strength for different graphene cluster models via natural bond order, and proposed a descriptor to quantitively represent the valence orbital level. This descriptor was defined as the difference between lowest valence orbital energy of the active center and the highest valence orbital energy of the entire graphene cluster (Fermi energy level in the form of natural atomic orbitals) (E_{diff}). They found that the adsorption energy of OH*, ΔG_{OH*} data plotted against E_{diff} formed a linear relationship for a wide variety of graphene active sites. Here, our calculations show that the adsorption free energies of O*, OH*, and OOH* are linearly proportional to Φ (Figure 2C), suggesting that Φ should be linearly correlated to E_{diff}. Therefore, Φ is intrinsically related to the valence orbital level, and consistent with the descriptor based on the orbital energy theory.[26]

Compared with the proposed descriptors such as orbital energy theory[26] and the work function,[27] Φ is more relevant to material properties and can be conveniently used to predict catalytic activity of doped carbon nanomaterials. For example, the

best catalyst is predicted to be the dopants with both affinity and electronegativity slightly higher than carbon (ratio ≈ 1.2). When the descriptor is small ($\Phi < 0.5$) the electronegativity dominates and the catalytic activity is low, whereas for $\Phi > 2.5$, the electron affinity gains in control, the activity is also low. This descriptor follows the Sabatier principle, which states that the interaction between the catalysts and the adsorbates should be neither too strong nor too weak, leading to the important new aspect of quantifying this interaction strength. Together with insights gained from the catalytic mechanism studies, the descriptor can be applied to guide the experiments to create active sites for highly efficient ORR and OER. This limited number of descriptors can then be used to screen candidate structures, and guide the experimental and computational search for highly efficient catalysts with single or dual dopants.

In conclusion, we have discovered an intrinsic descriptor that can well describe the ORR/OER activities of heteroatom-doped carbon nanomaterials as efficient catalysts in clean energy conversion and storage. By taking consideration of the combined effects of the electron affinity and the electronegativity of dopants on charge redistribution over the carbon surface, we have developed the design principles for enhancing the ORR/OER activity of p-orbital element-doped carbon nanomaterials. Our findings can be explained by competition between the ability to form covalent bonds with carbon and that to transfer electrons in the reaction, which reduce the overpotentials and stabilize the adsorbates, and hence the fast ORR/OER kinetics. This work shows that doping near the edge of graphene nanoribbons is a promising strategy in developing highly active metal-free carbon-based bifunctional catalysts for ORR and OER in energy conversion and storage devices, including fuel cells, metal–air batteries, and water-splitting systems. Considering the similarity of 2D materials, the descriptor and the approach developed in this study could also be applied for transition metal doped graphene or catalysts based on 2D materials beyond graphene.

Supporting Information

Supporting Information is available from the Wiley Online Library or from the author.

Acknowledgments

Z.Z., M.L., and L.Z. contributed equally to this work. This work is supported financially by Air Forces MURI program for the support of this research under Contract No. FA9550-12-1-0037 and the National Science Foundation (Grant Nos. NSF-AIR-IIP-1343270, NSF-CMMI-1363123). Computational resources were provided by UNT high-performance computing initiative.

Received: July 3, 2015
Revised: July 30, 2015
Published online: September 29, 2015

[1] a) B. Dunn, H. Kamath, J. M. Tarascon, *Science* **2011**, *334*, 928; b) Y. Tachibana, L. Vayssieres, J. R. Durrant, *Nat. Photonics* **2012**, *6*, 511.
[2] I. Katsounaros, S. Cherevko, A. R. Zeradjanin, K. J. J. Mayrhofer, *Angew Chem. Int. Ed.* **2014**, *53*, 102.
[3] C. Sealy, *Mater. Today* **2008**, *11*, 65.
[4] D. S. Su, G. Q. Sun, *Angew. Chem. Int. Ed.* **2011**, *50*, 11570.
[5] L. M. Dai, *Acc. Chem. Res.* **2013**, *46*, 31.
[6] D. Geng, Y. Chen, Y. Chen, Y. Li, R. Li, X. Sun, S. Ye, S. Knights, *Energy Environ. Sci.* **2011**, *4*, 760.
[7] a) Z.-H. Sheng, H.-L. Gao, W.-J. Bao, F.-B. Wang, X.-H. Xia, *J. Mater. Chem.* **2012**, *22*, 390; b) Z. Liu, X. Fu, M. Li, F. Wang, Q. Wang, G. Kang, F. Peng, *J. Mater. Chem. A* **2015**, *3*, 3289; c) S. Wang, L. Zhang, Z. Xia, A. Roy, D. W. Chang, J. B. Baek, L. Dai, *Angew. Chem.* **2012**, *51*, 4209.
[8] M. Park, T. Lee, B. S. Kim, *Nanoscale* **2013**, *5*, 12255.
[9] L. Yang, S. Jiang, Y. Zhao, L. Zhu, S. Chen, X. Wang, Q. Wu, J. Ma, Y. Ma, Z. Hu, *Angew. Chem.* **2011**, *50*, 7132.
[10] a) Z. W. Liu, F. Peng, H. J. Wang, H. Yu, W. X. Zheng, J. Yang, *Angew. Chem.* **2011**, *50*, 3257; b) C. Zhang, N. Mahmood, H. Yin, F. Liu, Y. Hou, *Adv. Mater.* **2013**, *25*, 4932.
[11] D. S. Yang, D. Bhattacharjya, S. Inamdar, J. Park, J. S. Yu, *J. Am. Chem. Soc.* **2012**, *134*, 16127.
[12] a) S. Yang, L. Zhi, K. Tang, X. Feng, J. Maier, K. Müllen, *Adv. Funct. Mater.* **2012**, *22*, 3634; b) L. T. Qu, Y. Liu, J. B. Baek, L. M. Dai, *ACS Nano* **2010**, *4*, 1321.
[13] a) Z. Yang, Z. Yao, G. F. Li, G. Y. Fang, H. G. Nie, Z. Liu, X. M. Zhou, X. Chen, S. M. Huang, *ACS Nano* **2012**, *6*, 205; b) Y. Zhang, M. Chu, L. Yang, W. Deng, Y. Tan, M. Ma, Q. Xie, *Chem. Commun.* **2014**, *50*, 6382.
[14] X. Sun, P. Song, T. Chen, J. Liu, W. Xu, *Chem. Commun.* **2013**, *49*, 10296.
[15] X. Sun, P. Song, Y. Zhang, C. Liu, W. Xu, W. Xing, *Sci. Rep.* **2013**, *3*, 2505.
[16] Z. Chen, D. Higgins, Z. Chen, *Carbon* **2010**, *48*, 3057.
[17] I. Y. Jeon, H. J. Choi, M. Choi, J. M. Seo, S. M. Jung, M. J. Kim, S. Zhang, L. Zhang, Z. Xia, L. Dai, N. Park, J. B. Baek, *Sci. Rep.* **2013**, *3*, 1810.
[18] D. Yu, Y. Xue, L. Dai, *J. Phys. Chem. Lett.* **2012**, *3*, 2863.
[19] Z. Yao, H. G. Nie, Z. Yang, X. M. Zhou, Z. Liu, S. M. Huang, *Chem. Commun.* **2012**, *48*, 1027.
[20] Z. Jin, H. Nie, Z. Yang, J. Zhang, Z. Liu, X. Xu, S. Huang, *Nanoscale* **2012**, *4*, 6455.
[21] K. P. Gong, F. Du, Z. H. Xia, M. Durstock, L. M. Dai, *Science* **2009**, *323*, 760.
[22] I. Y. Jeon, M. Choi, H. J. Choi, S. M. Jung, M. J. Kim, J. M. Seo, S. Y. Bae, S. Yoo, G. Kim, H. Y. Jeong, N. Park, J. B. Baek, *Nat. Commun.* **2015**, *6*, 7123.
[23] a) D. H. Lee, W. J. Lee, W. J. Lee, S. O. Kim, Y.-H. Kim, *Phys. Rev. Lett.* **2011**, *106*, 175502; b) U. N. Maiti, W. J. Lee, J. M. Lee, Y. Oh, J. Y. Kim, J. E. Kim, J. Shim, T. H. Han, S. O. Kim, *Adv. Mater.* **2014**, *26*, 40; c) W. J. Lee, U. N. Maiti, J. M. Lee, J. Lim, T. H. Han, S. O. Kim, *Chem. Commun.* **2014**, *50*, 6818; d) K. E. Lee, J. E. Kim, U. N. Maiti, J. Lim, J. O. Hwang, J. Shim, J. J. Oh, T. Yun, S. O. Kim, *ACS Nano* **2014**, *8*, 9073.
[24] B. Hammer, J. K. Norskov, *Nature* **1995**, *376*, 238.
[25] J. Suntivich, H. A. Gasteiger, N. Yabuuchi, H. Nakanishi, J. B. Goodenough, Y. Shao-Horn, *Nat. Chem.* **2011**, *3*, 546.
[26] Y. Jiao, Y. Zheng, M. Jaroniec, S. Z. Qiao, *J. Am. Chem. Soc.* **2014**, *136*, 4394.
[27] J. Y. Cheon, J. H. Kim, J. H. Kim, K. C. Goddeti, J. Y. Park, S. H. Joo, *J. Am. Chem. Soc.* **2014**, *136*, 8875.
[28] J. K. Norskov, J. Rossmeisl, A. Logadottir, L. Lindqvist, J. R. Kitchin, T. Bligaard, H. Jonsson, *J. Phys. Chem. B* **2004**, *108*, 17886.
[29] I. C. Man, H. Y. Su, F. Calle-Vallejo, H. A. Hansen, J. I. Martinez, N. G. Inoglu, J. Kitchin, T. F. Jaramillo, J. K. Norskov, J. Rossmeisl, *Chemcatchem* **2011**, *3*, 1159.
[30] H. Li, X. Cheng, F. B. Weng, A. Su, Y. C. Chiang, *J. Electrochem. Soc.* **2014**, *161*, F1140.
[31] L. Zhang, Z. Xia, *J. Phys. Chem. C* **2011**, *115*, 11170.
[32] a) W. J. Yuan, Y. Zhou, Y. R. Li, C. Li, H. L. Peng, J. Zhang, Z. F. Liu, L. M. Dai, G. Q. Shi, *Sci. Rep.* **2013**, *3*; b) A. Shen, Y. Zou, Q. Wang,

R. A. W. Dryfe, X. Huang, S. Dou, L. Dai, S. Wang, *Angew. Chem. Int. Ed.* **2014**, *53*, 10804.
[33] a) I.-Y. Jeon, H.-J. Choi, S.-M. Jung, J.-M. Seo, M.-J. Kim, L. Dai, J.-B. Baek, *J. Am. Chem. Soc.* **2013**, *135*, 1386; b) I. Y. Jeon, Y. R. Shin, G. J. Sohn, H. J. Choi, S. Y. Bae, J. Mahmood, S. M. Jung, J. M. Seo, M. J. Kim, D. W. Chang, L. M. Dai, J. B. Baek, *Proc. Natl. Acad. Sci. USA* **2012**, *109*, 5588.
[34] M. Li, L. Zhang, Q. Xu, J. Niu, Z. Xia, *J. Catal.* **2014**, *314*, 66.
[35] Z. Liu, F. Peng, H. Wang, H. Yu, J. Tan, L. Zhu, *Catal. Commun.* **2011**, *16*, 35.
[36] X. Sun, Y. Zhang, P. Song, J. Pan, L. Zhuang, W. Xu, W. Xing, *ACS Catal.* **2013**, *3*, 1726.
[37] H. Li, H. Liu, Z. Jong, W. Qu, D. Geng, X. Sun, H. Wang, *Int. J. Hydrogen Energy* **2011**, *36*, 2258.